Biotechnology Research and Innovation, 2025, 9(1): e2025001. https://doi.org/10.4322/biori.00012025

Biotechnology Research & Innovation

www.biori.periodikos.com.br

RESEARCH PAPERS

Rutile/anatase titanium dioxide nanocrystals enhance migration and proliferation of MC3T3-E1 pre-osteoblasts

Loyna Nobile Carvalho[a], Lucas Correia Peres[a], Anielle Christine Almeida Silva[b], Noelio Oliveira Dantas[b], Letícia de Souza Castro Filice[c], Vivian Alonso-Goulart[a,*]

[a]*Laboratory of Nanobiotechnology, Institute of Biotechnology – IBTEC, Federal University of Uberlândia – UFU, Uberlândia, MG, Brazil*
[b]*Laboratory of New Nanostructured and Functional Materials, Physics Institute, Federal University of Alagoas, Maceió, AL, Brazil*
[c]*Faculty of Medicine, Federal University of Uberlândia – UFU, Uberlândia, MG, Brazil*

Highlights

- TiO_2 NCs showed different phases depending on the heat treatment
- TiO_2 is not cytotoxic to MC3T3-E1 cells
- TiO_2 increased MC3T3-E1 cells proliferation and migration

Received 17 January, 2025; Accepted 21 July, 2025.

KEYWORDS
Regenerative medicine;
Titanium dioxide;
Migration;
Cytotoxicity.

Abstract: Alongside the development of biomaterials on a nanoscale, regenerative medicine is one of the most important areas of the 21st century. The combination of cells and nanomaterials can bring benefits such as tissue regeneration. Titanium dioxide is a well-researched metal that has numerous applications due to its unique properties compared to other metals. In this study, titanium dioxide nanocrystals in the anatase, rutile and brookite phases were synthesized and characterized. Viability, proliferation, and migration assays were performed on MC3T3-E1 cells using TiO_2 nanocrystals at different concentrations. The results show that the nanocrystals have high purity and different phases depending on the heat treatment at 650 °C and 800 °C. The different phases and concentrations of nanocrystals showed no cytotoxicity to the cells (viability above 70% for every condition) and increased cell proliferation (cell numbers almost tripling on day 4 relatively to day 2), with a focus on rutile/anatase TiO_2 at 100 µg/mL (RA100), which increased cell migration compared to the control in almost 15%. These findings suggest that rutile/anatase TiO_2; NCs may support bone regeneration by promoting pre-osteoblast proliferation and migration. Further studies on osteogenic differentiation and gene expression are warranted.

***Corresponding author.**
E-mail: alonso.goulart@ufu.br (V. Alonso-Goulart)

Graphical Abstract

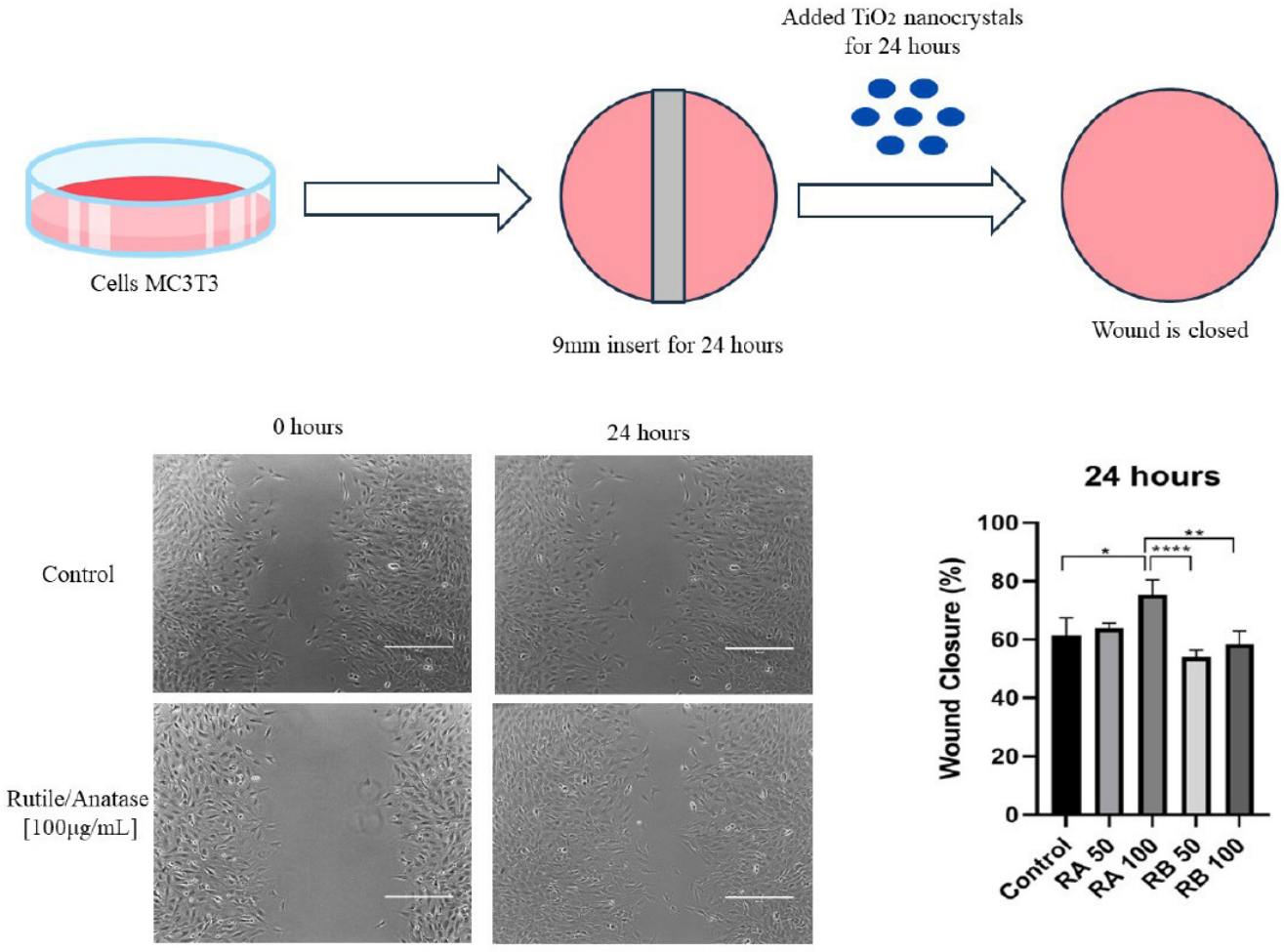

Introduction

Regenerative medicine seeks to restore, repair, or replace damaged tissues and organs through the integration of cells, biomaterials, and molecular biology when native healing is inadequate (Mao & Mooney, 2015; Sampogna et al., 2015). Traditional treatments such as organ transplants, allografts, and synthetic implants have helped address tissue loss from disease, trauma, or congenital conditions. However, these methods face critical limitations, including donor shortages, immune rejection, and surgical complications (Koria, 2012; Mizuno et al., 2012). For instance, although 36,761 transplants were performed in the U.S. in 2023, over 100,000 patients remain on waiting lists (United Network for Organ Sharing, 2022), highlighting the urgent need for alternative therapies. One such alternative is cell-based therapy, using autologous, allogeneic, or even xenogeneic cells such as chondrocytes, fibroblasts, or stem cells which can release signaling molecules that promote wound healing, cell proliferation, migration, and differentiation (Dzobo et al., 2018; Koria, 2012). To enhance the efficacy of these regenerative approaches, biomaterials, particularly at the nanoscale, are increasingly being explored.

The convergence of regenerative medicine with nanotechnology represents a major advancement (Yadav et al., 2022). Nanoparticles (NPs) particles ranging from 1 to 100 nm can serve as scaffolds or delivery systems for therapeutics. These include metallic NPs (e.g., gold, silver, titanium dioxide) known for their antibacterial and regenerative potential, and non-metallic NPs (e.g., silica, carbon-based materials), which are often employed for drug delivery or structural reinforcement (Akakuru et al., 2020; Mihai et al., 2019). Among these, titanium dioxide (TiO_2) stands out due to its versatility, low cost, and scalability. Commonly used in paints, cosmetics, sunscreens, and biomedical devices, TiO_2 nanoparticles are prized for their large surface area and enhanced physicochemical properties at the nanoscale (Alonso-Goulart et al., 2021; Javed et al., 2022). TiO_2 exists in three natural crystalline forms anatase, rutile, and brookite each with distinct properties affecting photocatalytic behavior, density, and stability (Eddy et al., 2023; Racovita, 2022). Anatase is most common, rutile is the most thermodynamically stable, and brookite is the least prevalent (Rashid et al., 2021).

However, these nanocrystals can pose toxicity risks. Their shape, size, and crystalline structure influence their reactivity and interaction with biological systems.

TiO_2 NPs may accumulate in organs such as the lungs, liver, and kidneys, potentially causing inflammation, oxidative stress (ROS), and cellular damage, including cytotoxicity, genotoxicity, and apoptosis (Yu et al., 2017). Despite these concerns, their antimicrobial properties remain promising for promoting wound healing, preventing infection, and targeting macrophages to induce M2 polarization an approach regarded as an effective strategy to enhance bone regeneration (Nikpasand & Parvizi, 2019; Wen et al., 2023).

Given these dual potentials—therapeutic and toxic—further research is essential. Particularly in cell-based regenerative strategies, there is a need to optimize nanoparticle concentration and phase composition to avoid adverse effects while enhancing healing. This study investigates, in vitro, the cytotoxic effects of TiO_2 nanocrystals (NCs) in the rutile/anatase and rutile/brookite phases, evaluating their influence on cell proliferation and migration at varying concentrations.

Material and methods

Synthesis and characterization of TiO_2 nanocrystals

The synthesis was carried out in aqueous solution at room temperature using a sol gel approach. Initially, 300 mL of ultrapure water was mixed with 60 mL of concentrated nitric acid (HNO_3, 70%, Sigma-Aldrich) and stirred magnetically for 20 minutes. Subsequently, 60 mL of titanium isopropoxide [$Ti(OCH(CH_3)_2)_4$, 97%, Sigma-Aldrich] was slowly added to the acidic solution. The solution was then left undisturbed to allow for the precipitation of TiO_2 nanocrystals. The resulting precipitate was redispersed in ultrapure water under magnetic stirring to ensure homogeneity and subsequently centrifuged at 6000 rpm for 10 minutes. The purified precipitate was thermally annealed in air under two distinct conditions: 650 °C for 1 h (sample RA – rutile/anatase) and 800 °C for 1 h (sample RB – rutile/brookite). The TiO_2 nanocrystals were synthesized via a sol-gel route using titanium isopropoxide, nitric acid, and NaOH. To enhance purity, the resulting material was thoroughly washed multiple times with deionized water and ethanol to remove residual precursors and byproducts. Although no specific endotoxin assay (e.g., LAL) was performed, all glassware and reagents were handled under aseptic conditions to minimize contamination.

Structural characterization was performed using X-ray diffraction (XRD) on a DRX-6000 diffractometer (Shimadzu, Shenzhen, China) equipped with monochromatic Cu $K\alpha_1$ radiation (λ = 1.54056 Å). The diffractograms confirmed the formation of crystalline TiO_2 and enabled the identification of anatase, rutile, and brookite phases (Leyva-Porras, 2015). The average crystallite sizes were estimated using the Debye–Scherrer equation (Guinier, 1963), yielding values of 32.0 nm for the RA sample and 44.1 nm for the RB sample. For both samples, size estimations were based on the full width at half maximum (FWHM) of the rutile (110) peak located at $2\theta \approx 27.8°$.

The relative mass fractions of anatase, rutile, and brookite were determined using established quantitative methods based on the intensities of selected characteristic peaks (Koo et al., 2006; Yu et al., 2003). Raman spectroscopy was also employed to further confirm the phase composition and vibrational properties of the TiO_2 nanocrystals. Raman spectra were recorded at room temperature using a LabRAM HR Evolution spectrometer (Horiba) equipped with a 633 nm excitation laser.

Cell culture

The cells used in all tests were MC3T3-E1 (ECACC 99072810). After thawing, the cells were cultured in 75cm² flasks in Minimum Essential Medium Alpha (α-MEM, Gibco™, Life Technologies, CA, USA) containing 10 vol% Fetal Bovine Serum (FBS, Cultilab, São Paulo, Brazil) and antibiotic-antimycotic 1 vol% (Gibco™, Life Technologies, CA, USA) herein referred to as complete medium. The culture medium was changed 2-3 times per week until the cells reached approximately 80% confluence. Passages 7-9 cells were used in all experiments.

Dispersion of TiO_2 NCs

The NC dispersion was prepared using a stock solution of TiO_2 in both phases RA and RB in ultrapure water at a concentration of 10 mg/mL. Then NCs were sonicated using a Q-Sonic ultrasonic disintegrator (700 W, 19-mm titanium tip) at 32 W for 10 minutes in pulse mode (8 s on, 2 s off) under ice bath cooling with an amplitude of 50%. NCs were prepared from RA and RB samples in a cell culture medium by diluting the stock solution in α-MEM supplemented with 10% (v/v) FBS, pH 7.4, at concentrations of 50 µg/mL or 100 µg/mL. These concentrations were selected based on the results of a previous study conducted by our research group (Duarte et al., 2020). Due to the increased aggregation of NCs in the culture medium, bovine serum albumin (BSA) was used as a stabilizing agent at a concentration of 100 µg/mL (Ribeiro et al., 2016).

Cell viability

The cell viability assay was performed using the Alamar blue assay, in which MC3T3-E1 cells were plated in a 96-well plate at a seeding density of $1x10^4$ cells per well. The plates were incubated overnight at 37 °C in a humidified atmosphere with 5% CO_2 to allow the cells to adhere to the surface. After the cell attachment period, the RA and RB NCs were added as a single dose for 24 hours at concentrations of 50 µg/mL or 100 µg/mL. As a positive control, cells were cultured in α-MEM 10% FBS medium. After 24 h of treatment with NCs, 20 µL of PBS containing resazurin (7-Hydroxy-3H-phenoxazin-3-one-10-oxide sodium salt) (Sigma-Aldrich, São Paulo, Brazil) (at a concentration of 0.3 µM) was added to each well. The plate was incubated for 4 h protected from ligh,t and then the absorbance was measured using a plate reader (EnSpire® Multimode Plate Reader - Massachusetts, USA) at 570 nm and 630 nm wavelengths. For analysis, the absorbance of the samples containing only α-MEM 10% FBS medium (no cells) was subtracted from the samples.

Cell proliferation

For the cell proliferation assay, cells were seeded in a 12-well plate at a density of $5x10^4$ cells per well and incubated overnight. Then, the culture medium was removed, and fresh

complete medium containing RA or RB NCs was added at concentrations of 50 µg/mL and 100 µg/mL as a single dose for 24 h. On day 0 (after 24 h of treatment), the culture medium was removed, cells were gently washed with PBS and then incubated with 500 µl of 0.25% trypsin/EDTA for 5 minutes at 37°C in a humidified atmosphere with 5% CO_2, detached cells were collected and centrifuged at 1500 rpm for 5 minutes. The pellet was resuspended in a complete medium. Trypan blue dye was used to count the cells in the Neubauer chamber. This procedure was repeated on days 2 and 4 after treatment.

Cell migration

Cell migration was performed using 0.9 mm-thick inserts (CytoSelect™, Cell Biolabs, San Diego, CA, USA). MC3T3-E1 Cells were seeded on a 24-well plate at a density of $1x10^5$ per well. The plate was incubated overnight at 37°C in a humidified atmosphere with 5% CO_2. The inserts and culture medium were then removed from the wells of the plate, and cells were treated with complete medium containing TiO_2 NCs in RA or RB phases at concentrations of 50 µg/mL or 100 µg/mL. The control group consisted of cells cultured in complete medium. After 24 h, the treatment was removed and replaced with fresh complete medium. Images were obtained at 0, 8, 24, 30, and 48 hours after the start of the treatment at 10x magnification using the EVOS microscope (Thermo Fisher Scientific, MA, USA). Images were analyzed using the Wound Healing Size Tool plugin in ImageJ software.

Statistical analysis

Statistical analyses were performed using GraphPad Prism 8.0 software (GraphPad Software, San Diego, USA). ANOVA-One-Way was used to compare the mean values of the cell viability assays, and ANOVA-Two-Way was used for the cell proliferation and migration assays ($P < 0.05$). All assays were performed in triplicate (n=3).

Results and discussion

Characterization of TiO_2 NCs

Figure 1 presents the XRD patterns of TiO_2 nanocrystals synthesized at two different thermal conditions: 650 °C/1 h and 800 °C/1 h. The diffraction peaks were indexed according to the Joint Committee on Powder Diffraction Standards (JCPDS) for anatase (JCPDS: 21-1272), rutile (JCPDS: 21-1276), and brookite (JCPDS: 29-1360), indicated by red (*), blue (**), and purple (***) symbols, respectively.

At 650 °C, the diffraction pattern (orange curve) revealed the coexistence of anatase and rutile phases. The prominent peak at 25.3° (2θ), corresponding to the (101) plane of anatase, and the presence of additional rutile peaks, such as that at 27.4° (2θ), attributed to the (110) plane, suggest a partial transformation of anatase into rutile. Quantitative phase analysis indicated that this sample (denoted RA) consisted of 35.44% anatase and 64.56% rutile, with an average crystallite size of 32 nm (Table 1).

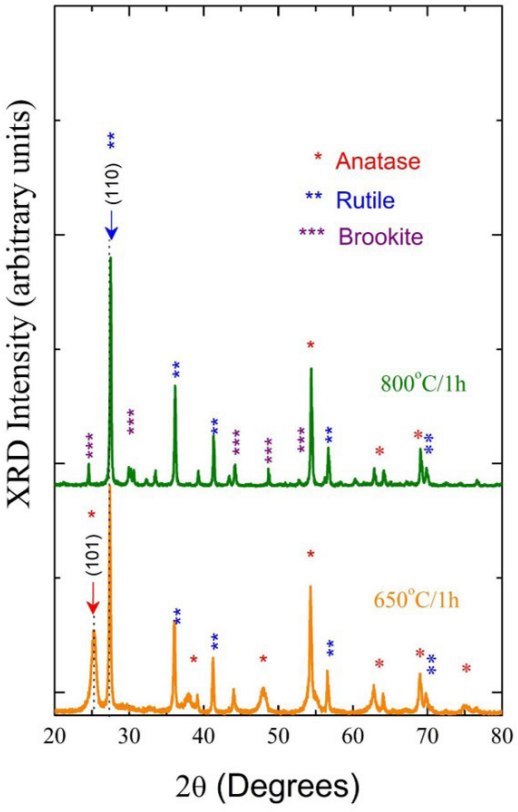

Figure 1. XRD patterns of samples subjected to annealing techniques 650°C/1h and 800°C/1h.

Table 1. Structural characteristics of TiO_2 nanocrystals synthesized at 650 °C and 800 °C for 1 hour. The samples RA and RB correspond to the mixed-phase compositions identified by XRD analysis. The data include the identified crystalline phases, calcination temperature, average crystallite size, and relative phase composition (%).

Name Sample	Crystalline Phases	Calcination Temperature (°C)	Average Crystallite Size (nm)	Relative Phase Composition (%)
RA	Rutile	650	32.0	64.50
	Anatase			35.44
RB	Rutile	800	44.1	84.07
	Brookite			15.90

The micro-Raman spectra of TiO_2 NCs exposed to thermal heating of 650ºC/1h and 800ºC/1h (Figure 2). All spectra were normalized to the highest intensity peak to facilitate visualization of the active micro-Raman modes. The Raman spectra of TiO_2 samples calcined at 650 °C and 800 °C for 1 h are shown in the Figure 2. The spectrum corresponding to the sample treated at 650 °C (orange curve) is dominated by vibrational modes attributed to the anatase phase, marked by red asterisks. The characteristic peaks of anatase are observed at approximately 144 cm^{-1} (E_g), 197 cm^{-1} (E_g), 399 cm^{-1} (B_{1g}), 519 cm^{-1} (A_{1g} + B_{1g}), and 639 cm^{-1} (E_g), which confirm the successful formation of this crystalline phase at lower temperatures.

In contrast, the Raman spectrum of the sample treated at 800 °C (green curve) shows significant spectral changes indicative of phase transformation. While anatase peaks are still detected, the appearance of new bands associated with rutile and brookite phases indicates a partial transition due to thermal treatment. The rutile phase (blue arrows) is confirmed by bands at approximately 447 cm^{-1} (E_g) and 612 cm^{-1} (A_{1g}), which are typical vibrational modes of its tetragonal structure.

Additionally, several peaks corresponding to the brookite phase (purple arrows) are observed, particularly at ~246, 321, 366, and 632 cm^{-1}. These bands can be assigned to the A_g and B_g vibrational modes of brookite, such as: 246 cm^{-1} (B_{1g}), 321 cm^{-1} (A_g), 366 cm^{-1} (B_{2g}), and 632 cm^{-1} (A_g). The co-existence of anatase, rutile, and brookite in the sample annealed at 800 °C suggests a thermally induced phase transformation pathway in which anatase progressively converts into the more thermodynamically stable rutile, with brookite appearing as a transient or intermediate phase. The presence of brookite, often rare in conventional syntheses, may be favored here by the nature of the green synthesis route, potentially influenced by residual phytochemicals or impurities acting as stabilizers.

These results underscore the importance of controlling calcination temperature to tailor the crystalline composition of TiO_2 nanomaterials. The ability to tune the proportion of TiO_2 polymorphs may offer distinct advantages in applications such as photocatalysis, antimicrobial coatings, and energy conversion, where phase-dependent properties are critical.

TiO2 is not cytotoxic to MC3T3-E1 cells

Determining the viability of cells is one of the most important parameters when testing a new biomaterial to ensure that it does not exhibit cytotoxicity. Part of the controversy surrounding TiO_2 is the different results regarding cytotoxicity. According to research by Santos-Aguilar et al. (2023), TiO_2 nanocrystals of different shapes and sizes can cause cell and tissue toxicity and accumulate in organs such as the lungs, liver, and kidneys, but can also affect the neurological system (Santos-Aguilar et al., 2023; Q. Yu et al., 2017).

Cell viability was analyzed after a single 24-h administration of TiO_2 NCs in the RA and RB phases at two concentrations of 50 µg/mL and 100 µg/mL. The assay performed was Alamar Blue, a metabolic assay utilizing the fluorimetric redox indicator resazurin, a non-fluorescent blue compound that is irreversibly reduced to resorufin by the process of aerobic respiration in viable cells, resulting in a color change to pink (Longhin et al., 2022).

RA and RB at concentrations of 50 and 100 µg/mL in cells for 24 h did not exhibit cytotoxicity (Figure 3), since according to ISO10993:5 (2009), only samples showing a reduction in viability of less than 70% are considered cytotoxic. Significant differences were detected among the treatment groups and when compared to the control. However, no significant difference was found between RA 50 µg/mL and the control, nor between RB 50 µg/mL and RB 100 µg/mL.

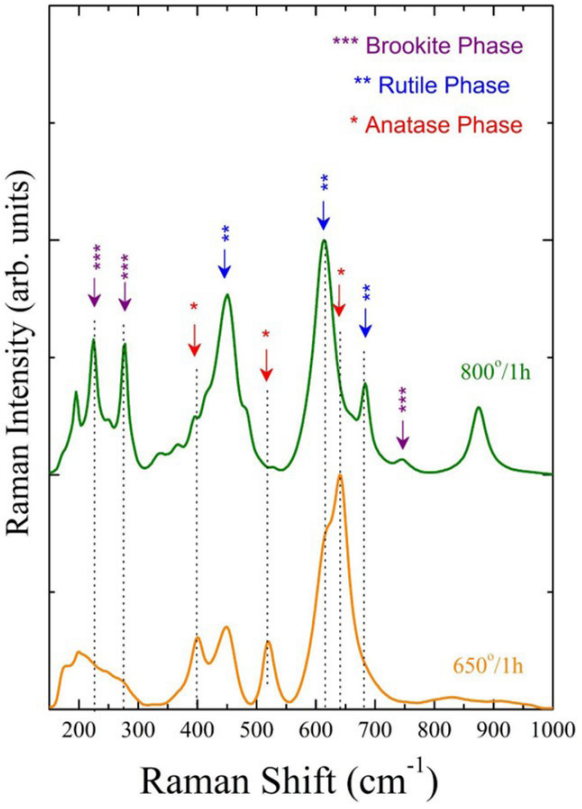

Figure 2. Micro Raman spectrum of TiO_2 NCs subjected to 650ºC / 1h and 800ºC / 1h.

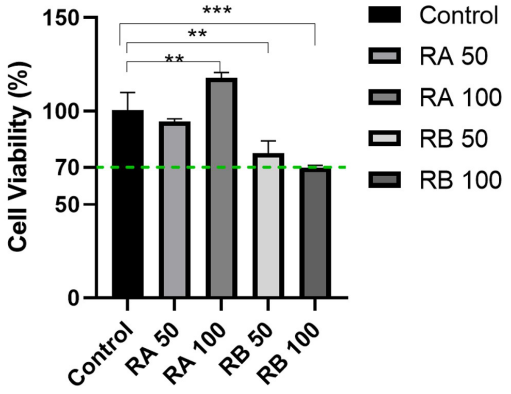

Figure 3. Alamar Blue Viability Assay of MC3T3-E1 Cells Exposed to TiO_2; NCs. Cell viability by alamar blue after 24 hours of treatment with NCs in the RA and RB phases at concentrations of 50 µg/mL and 100 µg/mL. Statistical analyses were evaluated using the ANOVA-One-Way method (** p= 0.001; *** p = 0.0001).

Studies such as that by Zhang et al. (2011) reported that the viability of the MC3T3 strain decreased when TiO_2 nanocrystals of different sizes were tested at concentrations of 50 µg/mL and 100 µg/mL after 24 h of treatment (Zhang et al., 2011). In Zhang's work, anatase nanocrystals of different sizes with a purity of 99% were used, while in this work, rutile/anatase and rutile/brookite nanocrystals were used, as shown in Table 1. This difference in the results can be attributed to the fact that anatase is more toxic due to its lower density, while the rutile phase exhibits greater stability among the three main phases (Akakuru et al., 2020).

Although the crystalline forms of TiO_2 NCs may be a substantial factor in the study of cytotoxicity, it is believed that the toxicity of TiO_2 NCs may also be related to their size, shape, surface coating, UV irradiation, and light exposure (Prokopiuk et al., 2023). For example, Dar et al. (2020) reported that studies conducted with NCs less than 20 nm in size can cause cytotoxicity and genotoxicity, in addition to impairing the immune system (Dar et al., 2020). This is consistent with our results, as the NCs used were 32 and 44.1 nm in size and did not show cytotoxicity.

According to the methodology of Ribeiro et al. (2016), the preparation of the NCs may have a significant impact on the viability results, as it aims to achieve better stability and homogeneity when the NCs are dispersed in a culture medium containing BSA, BSA proteins interact with the NC surface, forming a coating that prevents agglomeration and sedimentation of TiO_2. Duarte et al (2020) obtained similar non-cytotoxicity results in human adipose-derived mesenchymal stem cells with RA and RB NCs at the same concentrations when preparing the NCs with the same method, suggesting that the methodology is effective (Duarte et al., 2020; Santos-Aguilar et al., 2023). Beyond their biocompatibility, we observed that both RA and RB NCs notably increased MC3T3-E1 cell proliferation and migration.

TiO_2 increased MC3T3-E1 cells proliferation and migration

As shown in Figure 4, results of the cell proliferation assay on days 2 and 4 after 24 h of treatment with RA and RB NCs showed that on the second day, cell proliferation increased compared to the control, with RA 100 µg/mL, RB 50 µg/mL, and RB 100 µg/mL. By day 4, this proliferative effect was even more pronounced, with cell numbers almost tripling relative to day 2, showing a significant difference between the control group for all treatments, including RA 50 µg/mL, which had not shown a statistical difference on day 2.

The wound healing process involves complex factors such as hemostasis, which triggers the inflammatory response, recruitment of cells and cytokines, cell proliferation, and finally remodeling. Cell proliferation plays a fundamental role, as granulation tissue is formed during this phase, which contributes to the contraction of the extremities. Chemical mediators are released at the site of injury, signaling inflammatory cells to migrate to the injured tissue and close the wound, thereby restoring tissue integrity (Keely, 2013; Landén et al., 2016).

Analysis of percent wound closure in the cell migration assay revealed that after 24 h of treatment, wound closure of approximately 60% occurred in cells treated with RA 50 µg/mL and RB 100 µg/mL, while wound closure in RA 100 µg/mL was approximately 75%, representing substantially greater migration compared to control. There was also a significant difference between treatments, such as RA 100 µg/mL with RB 50 µg/mL and RA 100 µg/mL with RA 100 µg/mL, also showing greater cell migration, as shown in Figure 5A. After 30 hours of treatment, RA 100 µg/mL showed a migration percentage of approximately 80%, indicating a difference in wound closure compared to the control and RB 50 and 100 µg/mL. It is also observed that RA 50 µg/mL showed greater migration than RB 50 µg/mL, as presented in Figure 5B, and complete closure was observed across all treatment groups by 48 hours as shown in Figure 5C.

It was observed that the results of treatment with RB at 50 µg/mL showed low wound closure compared to the other treatments. In terms of cell migration, this treatment had the lowest performance in wound closure, with less than 60%, both in 24 and 30 hours, which is around 60%, while the other treatments are around 70% (Figure 6A).

The results on cell proliferation and migration obtained in this study are similar to those of Babitha and collaborators (2017). They demonstrate that the use of tetragonal TiO2 nanoparticles, less than 100 nm in size, in conjunction with polydopamine-zein scaffolds enhances both cell proliferation and migration of keratinocytes in vitro, compared to controls or scaffolds without TiO_2. Additionally, they demonstrated that TiO_2 has a significant impact on epidermal regeneration, as it accelerates wound healing in rats within 15 days compared to the control group (Babitha & Korrapati, 2017).

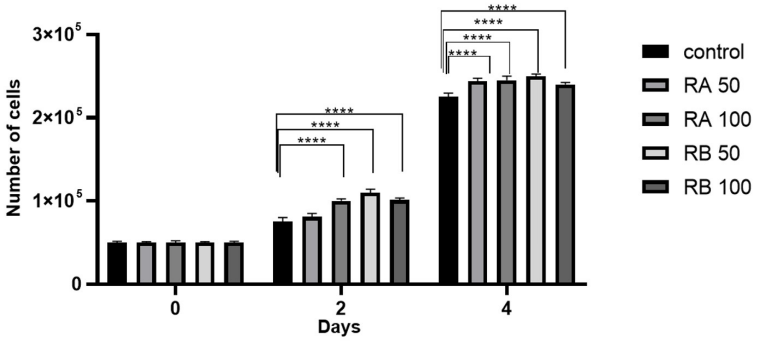

Figure 4. Effect of TiO2 RA and RB NCs on MC3T3-E1 cell proliferation over 4 days. A significant difference between control and treatments ($P < 0.0001$)

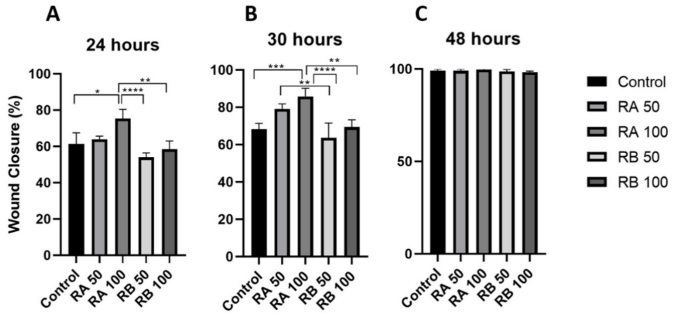

Figure 5. Cell migration using TiO_2 RA and RB. MC3T3-E1 cells were treated with TiO2 RA or RB NCs at concentrations of 50 µg/mL and 100 µg/mL. Migration was assessed after 24 hours (A), 30 hours (B) and 48h (C). A significant difference was observed between the control and RA 100 µg/mL and between treatments. (*p = 0.01; **p = 0.001; ***p = 0.001; ****p < 0.0001).

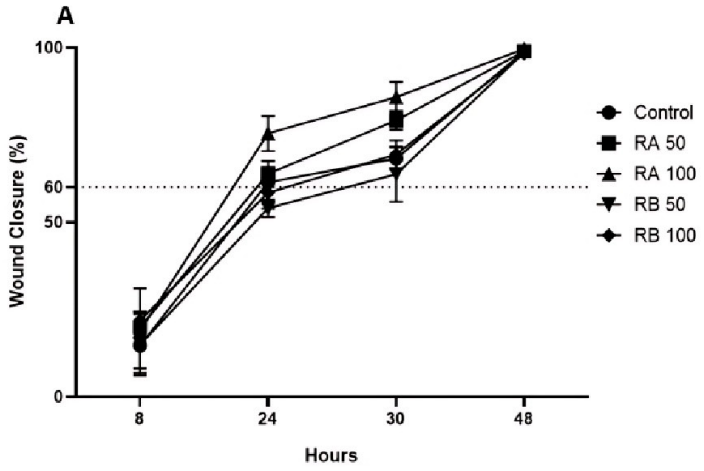

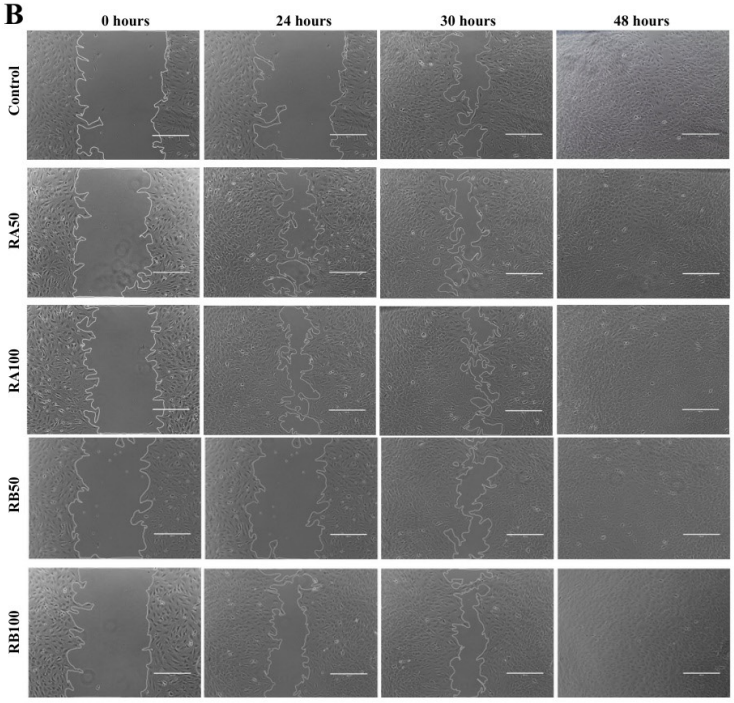

Figure 6. Time-course of MC3T3-E1 cell migration treated with TiO2 RA and RB NCs. Cell migration curve of NCs treatments at times 0, 8, 24, 30, and 48 hours (A). Images from the wound healing assay showing the migration of MC3T3 cells treated with TiO_2 RA and RB NCs at concentrations of 50 µg/mL and 100 µg/mL at times 0, 24, 30, and 48 hours, at 10X magnification (400 µm) on the Evos microscope (B).

Conclusion

This study demonstrates that TiO_2; nanocrystals in rutile/anatase and rutile/brookite phases, especially at 100 µg/mL, enhance MC3T3-E1 proliferation and migration without cytotoxic effects. These findings highlight the potential of TiO2; NCs in bone tissue engineering. Further studies assessing osteogenic differentiation and long-term cellular responses are warranted.

Conflict of interests

None

Funding

This research was supported by CAPES, CNPq, and FAPEMIG (grant numbers APQ-03613-17 and APQ-03063-16).

Acknowledgements

Luiz R. Goulart Filho, head of our laboratory and a prominent researcher, assisted us in carrying out this project with his unique suggestions, great inspiration, and relentless motivation.

References

Akakuru, O. U., Iqbal, Z. M., & Wu, A. (2020). TiO2 nanoparticles: Properties and applications. In A. Wu & W. Ren (Eds.), *TiO2 nanoparticles* (1st ed., pp. 1–66). Wiley. http://doi.org/10.1002/9783527825431.ch1

Alonso-Goulart, V., Carvalho, L. N., Marinho, A. L. G., De Oliveira Souza, B. L., De Aquino Pinto Palis, G., Lage, H. G. D., De Lima, I. L., Guimarães, L. D., Peres, L. C., Silveira, M. M., Lopes, G. H. N. L., Ferreira, L. B., & De Souza Castro-Filice, L. (2021). Biomaterials and adipose-derived mesenchymal stem cells for regenerative medicine: A systematic review. *Materials*, *14*(16), 4641. http://doi.org/10.3390/ma14164641. PMid:34443163.

Babitha, S., & Korrapati, P. S. (2017). Biodegradable zein-polydopamine polymeric scaffold impregnated with TiO2 nanoparticles for skin tissue engineering. *Biomedical Materials*, *12*(5), 055008. http://doi.org/10.1088/1748-605X/aa7d5a. PMid:28944761.

Dar, G. I., Saeed, M., & Wu, A. (2020). Toxicity of TiO2 nanoparticles. In A. Wu & W. Ren (Eds.), *TiO2 nanoparticles* (1st ed., pp. 67–103). Wiley. http://doi.org/10.1002/9783527825431.ch2

Duarte, C. A., Goulart, L. R., Filice, L. D. S. C., Lima, I. L. D., Campos-Fernández, E., Dantas, N. O., Silva, A. C. A., Soares, M. B. P., Santos, R. R. D., Cardoso, C. M. A., França, L. S. D. A., Rocha, V. P. C., Ribeiro, A. R. L. P., Perez, G., Carvalho, L. N., & Alonso-Goulart, V. (2020). Characterization of crystalline phase of TiO2 nanocrystals, cytotoxicity and cell internalization analysis on human adipose tissue-derived mesenchymal stem cells. *Materials*, *13*(18), 4071. http://doi.org/10.3390/ma13184071. PMid:32937776.

Dzobo, K., Thomford, N. E., Senthebane, D. A., Shipanga, H., Rowe, A., Dandara, C., Pillay, M., & Motaung, K. S. C. M. (2018). Advances in regenerative medicine and tissue engineering: innovation and transformation of medicine. *Stem Cells International*, *2018*, 2495848. http://doi.org/10.1155/2018/2495848. PMid:30154861.

Eddy, D. R., Permana, M. D., Sakti, L. K., Sheha, G. A. N., Solihudin, Hidayat, S., Takei, T., Kumada, N., & Rahayu, I. (2023). Heterophase polymorph of TiO2 (Anatase, Rutile, Brookite, TiO2 (B)) for efficient photocatalyst: fabrication and activity. *Nanomaterials*, *13*(4), 704. http://doi.org/10.3390/nano13040704. PMid:36839072.

Guinier, A., Lorrain, P., Lorrain, D. S.-M., e Gillis, J. (1964). X-Ray Diffraction Em Crystals, Imperfect Crystals, e Amorphous Bodies. Physics Today, 17(4), 70–72. http://doi.org/10.1063/1.3051547

Javed, R., Ain, N. U., Gul, A., Arslan Ahmad, M., Guo, W., Ao, Q., & Tian, S. (2022). Diverse Biotechnological Applications of Multifunctional Titanium Dioxide Nanoparticles: An up-to-date review. *IET Nanobiotechnology / IET*, 16(5), 171-189. http://doi.org/10.1049/nbt2.12085. PMid:35411585.

Keely, P. J. (2013). Cell migration within three-dimensional matrices. In W. J. Lennarz & M. D. Lane (Eds.), *Encyclopedia of biological chemistry* (pp. 436–445). Elsevier. http://doi.org/10.1016/B978-0-12-378630-2.00495-3

Koo, B., Park, J., Kim, Y., Choi, S.-H., Sung, Y.-E., & Hyeon, T. (2006). Simultaneous phase- and size-controlled synthesis of TiO2 nanorods via non-hydrolytic sol–gel reaction of syringe pump delivered precursors. *The Journal of Physical Chemistry B*, 110(48), 24318-24323. http://doi.org/10.1021/jp065372u. PMid:17134182.

Koria, P. (2012). Delivery of growth factors for tissue regeneration and wound healing. *BioDrugs*, 26(3), 163-175. http://doi.org/10.2165/11631850-000000000-00000. PMid:22500904.

Landén, N. X., Li, D., & Ståhle, M. (2016). Transition from inflammation to proliferation: A critical step during wound healing. *Cellular and Molecular Life Sciences*, 73(20), 3861-3885. http://doi.org/10.1007/s00018-016-2268-0. PMid:27180275.

Leyva-Porras, C., Toxqui-Teran, A., Vega-Becerra, O., Miki-Yoshida, M., Rojas-Villalobos, M., García-Guaderrama, M., & Aguilar-Martínez, J. A. (2015). Low-temperature synthesis and characterization of anatase TiO2 nanoparticles by an acid assisted sol–gel method. *Journal of Alloys and Compounds*, 647, 627-636. http://doi.org/10.1016/j.jallcom.2015.06.041.

Longhin, E. M., El Yamani, N., Rundén-Pran, E., & Dusinska, M. (2022). The alamar blue assay in the context of safety testing of nanomaterials. *Frontiers in Toxicology*, 4, 981701. http://doi.org/10.3389/ftox.2022.981701. PMid:36245792.

Mao, A. S., & Mooney, D. J. (2015). Regenerative medicine: Current therapies and future directions. *Proceedings of the National Academy of Sciences of the United States of America*, 112(47), 14452-14459. http://doi.org/10.1073/pnas.1508520112. PMid:26598661.

Mihai, M. M., Dima, M. B., Dima, B., & Holban, A. M. (2019). Nanomaterials for wound healing and infection control. *Materials*, 12(13), 2176. http://doi.org/10.3390/ma12132176. PMid:31284587.

Mizuno, H., Tobita, M., & Uysal, A. C. (2012). Concise review: Adipose-derived stem cells as a novel tool for future regenerative medicine. *Stem Cells*, 30(5), 804-810. http://doi.org/10.1002/stem.1076. PMid:22415904.

Nikpasand, A., & Parvizi, M. R. (2019). Evaluation of the effect of titatnium dioxide nanoparticles/gelatin composite on infected skin wound healing: An animal model study. *Bulletin of Emergency and Trauma*, 7(4), 366-372. http://doi.org/10.29252/beat-070405. PMid:31857999.

Prokopiuk, V., Yefimova, S., Onishchenko, A., Kapustnik, V., Myasoedov, V., Maksimchuk, P., Butov, D., Bespalova, I., & Tkachenko, A. (2023). Assessing the cytotoxicity of TiO2−x nanoparticles with a different Ti3+(Ti2+)/Ti4+ ratio. *Biological Trace Element Research*, 201(6), 3117-3130. http://doi.org/10.1007/s12011-022-03403-3. PMid:36029428.

Racovita, A. D. (2022). Titanium dioxide: Structure, impact, and toxicity. *International Journal of Environmental Research and Public Health*, 19(9), 5681. http://doi.org/10.3390/ijerph19095681. PMid:35565075.

Rashid, M. M., Forte Tavčer, P., & Tomšič, B. (2021). Influence of titanium dioxide nanoparticles on human health and the environment. *Nanomaterials*, 11(9), 2354. http://doi.org/10.3390/nano11092354. PMid:34578667.

Ribeiro, A. R., Gemini-Piperni, S., Travassos, R., Lemgruber, L. C., Silva, R., Rossi, A. L., Farina, M., Anselme, K., Shokuhfar, T., Shahbazian-Yassar, R., Borojevic, R., Rocha, L. A., Werckmann, J., & Granjeiro, J. M. (2016). Trojan-like internalization of anatase titanium dioxide nanoparticles by human osteoblast cells. *Scientific Reports*, 6(1), 23615. http://doi.org/10.1038/srep23615. PMid:27021687.

Sampogna, G., Guraya, S. Y., & Forgione, A. (2015). Regenerative medicine: Historical roots and potential strategies in modern medicine. *Journal of Microscopy and Ultrastructure*, 3(3), 101-107. http://doi.org/10.1016/j.jmau.2015.05.002. PMid:30023189.

Santos-Aguilar, P., Bernal-Ramírez, J., Vázquez-Garza, E., Vélez-Escamilla, L. Y., Lozano, O., García-Rivas, G. D. J., & Contreras-Torres, F. F. (2023). Synthesis and characterization of rutile TiO2 nanoparticles for the toxicological effect on the H9c2 cell line from rats. *ACS Omega*, 8(21), 19024-19036. http://doi.org/10.1021/acsomega.3c01771. PMid:37273591.

United Network for Organ Sharing. (2022, December 15). 2022 Organ Transplants again set annual records. https://unos.org/news/2022-organ-transplants-again-set-annual-records/

Wen, J., Cai, D., Gao, W., He, R., Li, Y., Zhou, Y., Klein, T., Xiao, L., & Xiao, Y. (2023). Osteoimmunomodulatory nanoparticles for bone regeneration. *Nanomaterials*, 13(4), 692. http://doi.org/10.3390/nano13040692. PMid:36839060.

Yadav, R., Dubey, A., Tiwari, S. P., Shrivastava, P., & Mandal, S. (2022). Nanotechnology and its applications: A scientific boon for future. *International Journal of Drug Delivery Technology*, 12(1), 1-8. http://doi.org/10.25258/ijddt.12.1.80.

Yu, J., Yu, J. C., Leung, M. K.-P., Ho, W., Cheng, B., Zhao, X., & Zhao, J. (2003). Effects of acidic and basic hydrolysis catalysts on the photocatalytic activity and microstructures of bimodal mesoporous titania. *Journal of Catalysis*, 217(1), 69-78. http://doi.org/10.1016/S0021-9517(03)00034-4.

Yu, Q., Wang, H., Peng, Q., Li, Y., Liu, Z., & Li, M. (2017). Different toxicity of anatase and rutile Tio 2 nanoparticles on macrophages: Involvement of difference in affinity to proteins and phospholipids. *Journal of Hazardous Materials*, 335, 125-134. http://doi.org/10.1016/j.jhazmat.2017.04.026. PMid:28437696.

Zhang, Y., Yu, W., Jiang, X., Lv, K., Sun, S., & Zhang, F. (2011). Analysis of the cytotoxicity of differentially sized titanium dioxide nanoparticles in murine MC3T3-E1 preosteoblasts. *Journal of Materials Science. Materials in Medicine*, 22(8), 1933-1945. http://doi.org/10.1007/s10856-011-4375-7. PMid:21681655.